Composite Structures 94 (2012) 415–422

Contents lists available at SciVerse ScienceDirect

Composite Structures

journal homepage: www.elsevier.com/locate/compstruct

Refined shell elements for the analysis of functionally graded structures

M. Cinefra [a,*,1], E. Carrera [a,2], L. Della Croce [b,3], C. Chinosi [c,3]

[a] Department of Aeronautics and Space Engineering, Politecnico di Torino, Torino, Italy
[b] Department of Mathematics, Universitá di Pavia, Pavia, Italy
[c] Department of Sciences and Advanced Technologies, Universitá del Piemonte Orientale, Alessandria, Italy

ARTICLE INFO

Article history:
Available online 25 August 2011

Keywords:
Functionally graded materials
Unified Formulation
Finite element method
Plates and shells
Mechanical load

ABSTRACT

The present paper considers the static analysis of plates and shells made of Functionally Graded Material (FGM), subjected to mechanical loads. Refined models based on the Carrera's Unified Formulation (CUF) are employed to account for grading material variation in the thickness direction. The governing equations are derived from the Principle of Virtual Displacement (PVD) in order to apply the Finite Element Method (FEM). A nine-nodes shell element with exact cylindrical geometry is considered. The shell can degenerate in the plate element by imposing an infinite radius of curvature. The Mixed Interpolation of Tensorial Components (MITC) technique is extended to the CUF in order to contrast the membrane and shear locking phenomenon. Different thickness ratios and orders of expansion for the displacement field are analyzed. The FEM results are compared with both benchmark solutions from literature and the results obtained using the Navier method that provides the analytical solution for simply-supported structures subjected to sinusoidal pressure loads. The shell element based on refined theories of the CUF turns out to be very efficient and its use is mandatory with respect to the classical models in the study of FGM structures.

1. Introduction

It is well known that many structural components, such as hollow cylinder, thin-walled shell, pipe and cylindrical panel undergo mechanical and/or thermal loads which may induce undesirable stresses and deformation. How to reduce the aforementioned stresses and deformation becomes important for engineering applications, and extensive effects have been devoted to this field [1]. Functionally Graded Materials (FGMs) as a new kind of composites were initially designed as thermal barrier materials for aerospace structures, in which the volume fractions of different material constituents vary continuously in one or more directions [2,3]. These novel nonhomogeneous materials have excellent thermo-mechanical properties and their use can eliminate and/or control the deformation of structural components [4]. For these reasons, the functionally graded materials have extensive applications to important structures, such as aerospace, nuclear reactors and chemical plants. This implies the necessity of an exhaustive analysis of structures made of FGM.

In recent years, several works have been devoted to the development of accurate structural models for FGM plates and shells. Some analytical solutions have been provided in literature for functionally graded bi-dimensional structures with arbitrary variation of the material properties along the thickness and subjected to mechanical and thermal loads [5–7]. Other researchers have adapted classical models, such as the Classical Lamination Theory (CLT) [8] and the First-order Shear Deformation Theory (FSDT) [9–11] to the analysis of functionally graded plates. Several finite element results are also provided in these cases. Pelletier and Vel [12] have been analyzed functionally graded cylindrical shells using the Flugge and the Donnell shell theories. In [13], mixed-interpolated finite elements have been used to study cylindrical shells made of functionally graded materials and the governing equations have been determined using the Naghdi theory. However, the accuracy of classical models is very limited because the assumption of constant transverse deflection through the thickness direction is not valid in functionally graded structures. Therefore, Ramirez et al. [14] have performed the static analysis of FGM plates by means of a discrete layer approach. Shao and Wang [15] have derived a series solution for a functionally graded hollow cylinder using a multi-layered approach based on the laminated composite theory. A third-order shear deformation theory has been developed by Ferreira et al. in [16] and the collocation with multi-quadric

* Corresponding author. Address: Department of Aeronautic and Space Engineering, Politecnico di Torino, Corso Duca degli Abruzzi 24, 10129 Torino, Italy. Tel.: +39 011 090 6869; fax: +39 011 090 6899.
E-mail addresses: maria.cinefra@polito.it (M. Cinefra), erasmo.carrera@polito.it (E. Carrera), lucia.dellacroce@unipv.it (L. Della Croce), claudia.chinosi@mfn.unipmn.it (C. Chinosi).
[1] PhD Student.
[2] Professor of Aerospace Structures and Computational Aeroelasticity.
[3] Professor of Mathematics.

0263-8223/$ - see front matter © 2011 Elsevier Ltd. All rights reserved.
doi:10.1016/j.compstruct.2011.08.006

radial basis functions has been used to evaluate the static response of FGM plates. In [17], Qian et al. have combined a higher-order shear and normal deformable plate theory with the local meshless Petrov–Galerkin method [18] for the static and dynamic analysis of FGM plates. In these last cases, the obtained results show the importance to adopt higher-order models for the analysis of FGM structures.

For this aim the Carrera's Unified Formulation (CUF), which was developed by Carrera for multi-layered structures [19], has been extended to functionally graded structures. Several refined and advanced hierarchical two-dimensional models have been developed using the CUF, that have the order of expansion for the primary variables in the thickness direction as free parameter. The CUF analytical solutions of the thermo-mechanical and dynamic analysis of FGM plates and shells have been presented in [20–24]. In these works, the Principle of Virtual Displacements (PVD) has been proposed to derive the governing equations. While, the extension of Reissner's Mixed Variational Theorem (RMVT) to multilayered structures embedding FGM layers has been given in [25,26]. The obtained results were in good agreement with the reference solutions and they showed that the use of higher-order expansions is mandatory for FGMs, especially in the thermal analysis.

In order to analyze FGM structures with arbitrary boundary conditions and subjected to general loads, a shell finite element based on the Unified Formulation is here proposed. Some FEM models have been already proposed for the study of FGM plates and shells [27–29], but they are based on the classical theories. The present shell element can employ all the refined higher-order models contained in the Unified Formulation. It has cylindrical geometry and it adopts the Mixed Interpolation of Tensorial Components (MITC) method to overcome the locking phenomenon. Plate models can be also considered by imposing the radius of curvature of the cylinder to be infinite. The governing equations are derived from the PVD and the constitutive equations take into account the continuous variability of elastic properties of the material in the thickness direction. The results are compared with benchmark solutions from both the literature and the CUF analytical solutions presented in [21,22]. The thermal analysis of FGM plates and shells will be presented in a companion future work.

2. Refined models via Unified Formulation

The main feature of the Unified Formulation by Carrera (CUF) [30] is the unified manner in which the displacement variables are handled. According to CUF, the displacement field is written by means of 2D-expansion functions in the thickness direction as follows:

$$\begin{aligned}&\delta\boldsymbol{u}(\xi_1,\xi_2,\xi_3) = F_\tau(\xi_3)\delta\boldsymbol{u}_\tau(\xi_1,\xi_2),\\&\boldsymbol{u}(\xi_1,\xi_2,\xi_3) = F_s(\xi_3)\boldsymbol{u}_s(\xi_1,\xi_2), \quad \tau,\ s = 0,1,\ldots,N,\end{aligned} \tag{1}$$

where $\boldsymbol{u} = \{u, v, w\}$, δ indicates the virtual variation and k identifies the layer. (ξ_1,ξ_2,ξ_3) is a curvilinear coordinates system placed at the center of the upper part of the midsurface of the shell as shown in Fig. 1. F_τ and F_s are the so-called thickness functions depending only on the thickness coordinate ξ_3. $\boldsymbol{u}_s$ are the unknown variables depending on the coordinates ξ_1 and ξ_2. τ and s are sum indexes and N is the order of expansion in the thickness direction assumed for the displacements.

A Taylor expansion is employed as thickness functions in order to obtain refined models. Therefore, the displacement field reads:

$$\boldsymbol{u}^k = F_0\,\boldsymbol{u}_0^k + F_1\,\boldsymbol{u}_1^k + \ldots + F_N\,\boldsymbol{u}_N^k = F_s\,\boldsymbol{u}_s^k, \quad s = 0,1,\ldots,N, \tag{2}$$

$$F_0 = \xi_3^0 = 1, \quad F_1 = \xi_3^1 = \xi_3, \quad \ldots, \quad F_N = \xi_3^N. \tag{3}$$

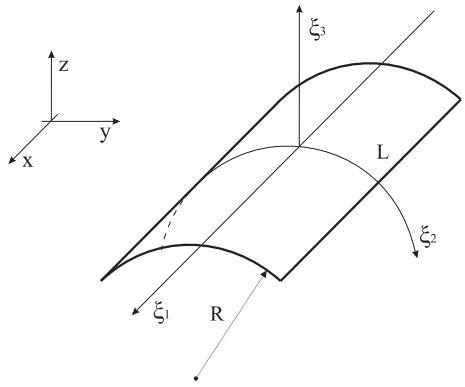

Fig. 1. Curvilinear coordinates reference system.

$N = 4$ is usually taken as maximum order of expansion because it is enough to guarantee the convergence of the solution. Classical theories, such as the First-order Shear Deformation Theory (FSDT), can be obtained from a first-order model ($N = 1$), by imposing a constant transverse displacement through the thickness via penalty techniques. For more details about the Unified Formulation the readers can refer to [19,30].

3. Shell element with cylindrical geometry

In this work a shell element with exact cylindrical geometry is considered. Using the linear part of the 3D Green–Lagrange tensor as shown in [31], one can obtain the following strain–displacement relations expressed in the curvilinear reference system (ξ_1,ξ_2,ξ_3):

$$\begin{aligned}\varepsilon_{11} &= F_\tau u_{\tau,1}\\ \varepsilon_{22} &= F_\tau\left[\left(1+\frac{\xi_3}{R}\right)\frac{w_\tau}{R} + \left(1+\frac{\xi_3}{R}\right)v_{\tau,2}\right]\\ \varepsilon_{12} &= F_\tau\left[u_{\tau,2} + \left(1+\frac{\xi_3}{R}\right)v_{\tau,1}\right]\\ \varepsilon_{13} &= w_{\tau,1}F_\tau + u_\tau F_{\tau,3}\\ \varepsilon_{23} &= F_\tau\left[w_{\tau,2} - \frac{v_\tau}{R}\right] + F_{\tau,3}\left[\left(1+\frac{\xi_3}{R}\right)v_\tau\right]\\ \varepsilon_{33} &= w_\tau F_{\tau,3}\end{aligned} \tag{4}$$

where R is the radius of the cylinder taken in the ξ_2-direction (see Fig. 1). The Unified Formulation has been applied to the displacements. The comma indicates the derivative with respect to the coordinates ξ_1, ξ_2 or ξ_3.

For convenience, the geometrical relations can be expressed in matrix form as:

$$\begin{aligned}\boldsymbol{\varepsilon}_p &= (\boldsymbol{D}_p + \boldsymbol{A}_p)\boldsymbol{u}\\ \boldsymbol{\varepsilon}_n &= (\boldsymbol{D}_{n\Omega} + \boldsymbol{D}_{nz} - \boldsymbol{A}_n)\boldsymbol{u}\end{aligned} \tag{5}$$

where the strains have been arranged in the vectors $\boldsymbol{\varepsilon}_p = \{\varepsilon_{11},\varepsilon_{22},\varepsilon_{12}\}$ and $\boldsymbol{\varepsilon}_n = \{\varepsilon_{13},\varepsilon_{23},\varepsilon_{33}\}$, and the differential operators are defined as follows:

$$\boldsymbol{D}_p = \begin{bmatrix}\partial_1 & 0 & 0\\ 0 & H\partial_2 & 0\\ \partial_2 & H\partial_1 & 0\end{bmatrix}, \quad \boldsymbol{D}_{n\Omega} = \begin{bmatrix}0 & 0 & \partial_1\\ 0 & 0 & \partial_2\\ 0 & 0 & 0\end{bmatrix},$$

$$\boldsymbol{D}_{nz} = \partial_3 \cdot \boldsymbol{A}_{nz} = \partial_3\begin{bmatrix}1 & 0 & 0\\ 0 & H & 0\\ 0 & 0 & 1\end{bmatrix}, \tag{6}$$

$$\boldsymbol{A}_p = \begin{bmatrix}0 & 0 & 0\\ 0 & 0 & \frac{1}{R}H\\ 0 & 0 & 0\end{bmatrix}, \quad \boldsymbol{A}_n = \begin{bmatrix}0 & 0 & 0\\ 0 & \frac{1}{R} & 0\\ 0 & 0 & 0\end{bmatrix}, \tag{7}$$

in which $H = \left(1 + \frac{\xi_3}{R}\right)$ and the matrix $\boldsymbol{A}_{n_z}$ is introduced. For more details about the derivation of the geometrical relations one can refer to [31,32]. One can note that the above geometrical relations are valid for the plate if the condition $\frac{1}{R} = 0$ is imposed.

According to the FEM, the displacement components can be interpolated on the nodes of the element by means of the Lagrangian shape functions N_i as follows:

$$\delta\boldsymbol{u}_\tau = N_i \delta\boldsymbol{q}_{\tau_i}, \quad \boldsymbol{u}_s = N_j \boldsymbol{q}_{s_j}, \tag{8}$$

where $i, j = 1, \ldots, 9$ by considering a nine-nodes element. $\boldsymbol{q}_{s_j}$ and $\delta\boldsymbol{q}_{\tau_i}$ are the nodal displacement components and their virtual variations. Therefore, substituting these expressions in the geometrical relations (5), one has:

$$\begin{aligned} \boldsymbol{\varepsilon}_p &= F_\tau(\boldsymbol{D}_p + \boldsymbol{A}_p)(N_i\boldsymbol{I})\boldsymbol{q}_{\tau_i} \\ \boldsymbol{\varepsilon}_n &= F_\tau(\boldsymbol{D}_{n\Omega} - \boldsymbol{A}_n)(N_i\boldsymbol{I})\boldsymbol{q}_{\tau_i} + F_{\tau,3}\boldsymbol{A}_{nz}(N_i\boldsymbol{I})\boldsymbol{q}_{\tau_i} \end{aligned} \tag{9}$$

where $\boldsymbol{I}$ is a 3×3 identity matrix.

4. MITC method extended to nine-nodes elements

Considering the strains in the local coordinate system (ξ, η), the MITC shell elements ([33,34]) are formulated by using, instead of the strain components directly computed from the displacements, an interpolation of these strain components within each element using a specific interpolation strategy for each component. The corresponding interpolation points, called tying points, are shown in Fig. 2 for a nine-nodes element.

The interpolating functions on tying points can be arranged in the following arrays:

$$\begin{aligned} N_{m1} &= [N_{A1}, N_{B1}, N_{C1}, N_{D1}, N_{E1}, N_{F1}] \\ N_{m2} &= [N_{A2}, N_{B2}, N_{C2}, N_{D2}, N_{E2}, N_{F2}] \\ N_{m3} &= [N_P, N_Q, N_R, N_S] \end{aligned} \tag{10}$$

For convenience, the subscripts $m1$, $m2$ and $m3$ will indicate quantities calculated in the points (A1, B1, C1, D1, E1, F1), (A2, B2, C2, D2, E2, F2) and (P, Q, R, S), respectively. Therefore, the strain components are interpolated as follows:

$$\begin{aligned} \boldsymbol{\varepsilon}_p &= \begin{bmatrix} \varepsilon_{11} \\ \varepsilon_{22} \\ \varepsilon_{12} \end{bmatrix} = \begin{bmatrix} N_{m1} & 0 & 0 \\ 0 & N_{m2} & 0 \\ 0 & 0 & N_{m3} \end{bmatrix} \begin{bmatrix} \varepsilon_{11_{m1}} \\ \varepsilon_{22_{m2}} \\ \varepsilon_{12_{m3}} \end{bmatrix} \\ \boldsymbol{\varepsilon}_n &= \begin{bmatrix} \varepsilon_{13} \\ \varepsilon_{23} \\ \varepsilon_{33} \end{bmatrix} = \begin{bmatrix} N_{m1} & 0 & 0 \\ 0 & N_{m2} & 0 \\ 0 & 0 & 1 \end{bmatrix} \begin{bmatrix} \varepsilon_{13_{m1}} \\ \varepsilon_{23_{m2}} \\ \varepsilon_{33} \end{bmatrix} \end{aligned} \tag{11}$$

where the strains $\varepsilon_{11_{m1}}$, $\varepsilon_{22_{m2}}$, $\varepsilon_{12_{m3}}$, $\varepsilon_{13_{m1}}$, $\varepsilon_{23_{m2}}$ are expressed by means of Eq. (9), in which the shape functions N_i are calculated in the tying points. More details about the MITC9 shell element are given in [32].

5. Constitutive equations for FGMs

According to the notation used above, the constitutive equations read as follows:

$$\begin{aligned} \boldsymbol{\sigma}_p &= \boldsymbol{C}_{pp}\ \boldsymbol{\epsilon}_p + \boldsymbol{C}_{pn}\ \boldsymbol{\epsilon}_n \\ \boldsymbol{\sigma}_n &= \boldsymbol{C}_{np}\ \boldsymbol{\epsilon}_p + \boldsymbol{C}_{nn}\ \boldsymbol{\epsilon}_n \end{aligned} \tag{12}$$

where $\boldsymbol{\sigma}_p = \{\sigma_{11}, \sigma_{22}, \sigma_{12}\}$ and $\boldsymbol{\sigma}_n = \{\sigma_{13}, \sigma_{23}, \sigma_{33}\}$. The Eq. (12) are obtained using the well-known Hooke's law.

In the case of functionally graded materials, the properties change continuously along a particular direction of the plate or shell. In this work, the matrices of elastic coefficients are assumed to be dependent on the thickness coordinate ξ_3 and they are:

$$\begin{aligned} \boldsymbol{C}_{pp} &= \begin{bmatrix} C_{11} & C_{12} & 0 \\ C_{12} & C_{11} & 0 \\ 0 & 0 & C_{44} \end{bmatrix}, \quad \boldsymbol{C}_{pn} = \begin{bmatrix} 0 & 0 & C_{12} \\ 0 & 0 & C_{12} \\ 0 & 0 & 0 \end{bmatrix}, \\ \boldsymbol{C}_{np} &= \begin{bmatrix} 0 & 0 & 0 \\ 0 & 0 & 0 \\ C_{12} & C_{12} & 0 \end{bmatrix}, \quad \boldsymbol{C}_{nn} = \begin{bmatrix} C_{44} & 0 & 0 \\ 0 & C_{44} & 0 \\ 0 & 0 & C_{11} \end{bmatrix}, \end{aligned} \tag{13}$$

in which:

$$\begin{aligned} C_{11}(\xi_3) &= \frac{E(1-\nu)}{(1+\nu)(1-2\nu)} \\ C_{12}(\xi_3) &= \frac{E\nu}{(1+\nu)(1-2\nu)} \\ C_{44}(\xi_3) &= \frac{E}{2(1+\nu)} \end{aligned} \tag{14}$$

The Young modulus $E = E(\xi_3)$ and the Poisson ratio $\nu = \nu(\xi_3)$ are general continuous functions of the thickness coordinate, according to a given material law.

6. Governing equations

This section presents the derivation of the finite element stiffness matrix based on the Principle of Virtual Displacement (PVD) according to the Unified Formulation and the MITC method.

In general, the PVD for a bi-dimensional structure reads:

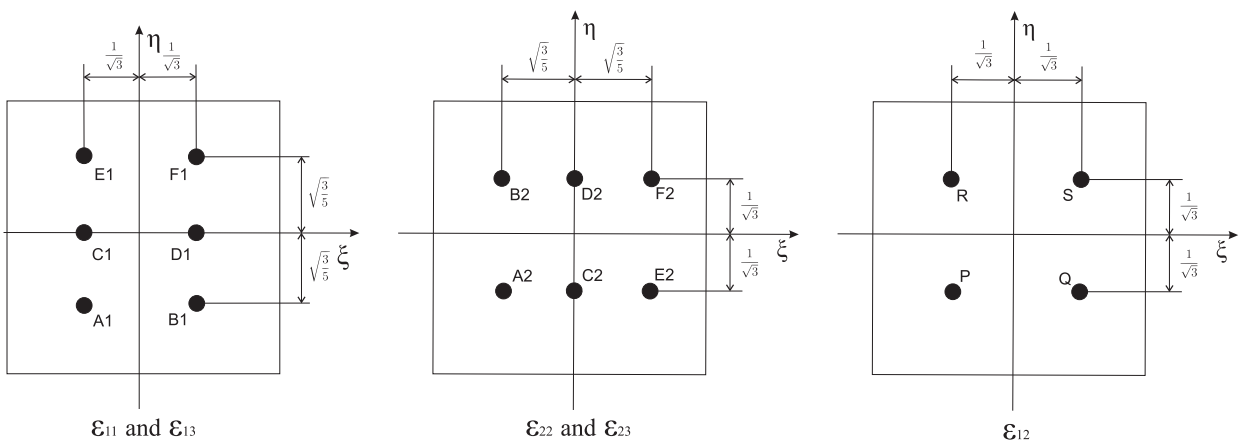

Fig. 2. Interpolation strategy for strain components.

$$\int_\Omega \int_A \left\{ \delta \boldsymbol{\varepsilon}_p^T \boldsymbol{\sigma}_p + \delta \boldsymbol{\varepsilon}_n^T \boldsymbol{\sigma}_n \right\} d\Omega\, dz = \int_\Omega \int_A \{ \delta \boldsymbol{u}\boldsymbol{p} \}\, d\Omega\, dz \tag{15}$$

where Ω and A are the integration domains in the plane and in the thickness direction, respectively. The first member of the equation represents the variation of the internal work, while the second member is the external work. $\boldsymbol{p} = \boldsymbol{p}(\xi_1, \xi_2, \xi_3)$ is the mechanical load applied to the structure.

In the case of the shell, one needs to refer the integration domains to the curvilinear reference system (ξ_1, ξ_2, ξ_3). Therefore, the parameter H, defined in the Section 3 for the cylindrical geometry, is introduced in the PVD as follows:

$$\int_\Omega \int_A \left\{ \delta \boldsymbol{\varepsilon}_p^T \boldsymbol{\sigma}_p + \delta \boldsymbol{\varepsilon}_n^T \boldsymbol{\sigma}_n \right\} H\, d\Omega\, d\xi_3 = \int_\Omega \int_A \{ \delta \boldsymbol{u}\ \boldsymbol{p} \} H\, d\Omega\, d\xi_3 \tag{16}$$

remembering that H assumes the value 1 in the case of plate.

Substituting the constitutive Eqs. (12), the geometrical relations written via the MITC method (11) in the PVD Eq. (16) and applying the Unified Formulation (1) and the FEM approximation (8), one obtains the following governing equations:

$$\delta \boldsymbol{q}_{\tau_i} : \boldsymbol{K}^{\tau s\, ij} \boldsymbol{q}_{s_j} = \boldsymbol{P}_{\tau_i} \tag{17}$$

where $\boldsymbol{K}^{\tau s\ i\ j}$ is a 3×3 matrix, called fundamental nucleus, is the basic element from which the stiffness matrix of the whole structure is computed, while $\boldsymbol{P}_{\tau i}^k$ is the fundamental nucleus for the vector of nodal loads. For more details about the expansion of fundamental nuclei on the indexes τ,s and i, j one can refer to [30].

For the sake of clarity, the explicit form of the fundamental nucleus $\boldsymbol{K}^{\tau s\ i\ j}$ is presented in the Appendix.

7. Numerical results and discussion

As a typical example for high-temperature applications, the constituent materials of the functionally graded structure are taken to be Monel (70Ni–30Cu), a nickel-based alloy, and the ceramic zirconia (ZrO_2). The required material properties are those reported in [35]:

$$B_m = 227.24\ \text{GPa}, \quad \mu_m = 65.55\ \text{GPa}, \quad \alpha_m = 15 \times 10^{-6}/\text{K}, \quad K_m = 25\ \text{W/mK}, \quad \text{for Monel},$$
$$B_c = 125.83\ \text{GPa}, \quad \mu_c = 58.08\ \text{GPa}, \quad \alpha_c = 10 \times 10^{-6}/\text{K}, \quad K_c = 2.09\ \text{W/mK}, \quad \text{for zirconia}.$$

For this two-phase composite material different micromechanical models can be applied for the computation of the effective local material properties. According to [35], the following formulas are chosen:

- The effective bulk modulus B and shear modulus μ are given by the mean field estimate of Mori and Tanaka [36,37]:

$$\frac{B - B_m}{B_c - B_m} = \frac{V_2}{1 + (1 - V_2)\frac{B_c - B_m}{B_m + \frac{4}{3}\mu_m}} \tag{18}$$

$$\frac{\mu - \mu_m}{\mu_c - \mu_m} = \frac{V_2}{1 + (1 - V_2)\frac{\mu_c - \mu_m}{\mu_m + f_1}} \quad \text{with} \quad f_1 = \frac{\mu_m(9B_m + 8\mu_m)}{6(B_m + 2\mu_m)} \tag{19}$$

In Eqs. (18), the indices m and c refer to the metallic and ceramic phase, respectively. V_2 is the volume fraction of the ceramic phase that is assumed for the computations as:

$$V_2 = V_c = \left(\frac{\xi_3}{h} \right)^{n_g} \tag{20}$$

where by changing the exponent n_g different material gradients can be accomplished. Fig. 3 shows the through-thickness distribution of the volume fraction V_c of the ceramic phase and the resulting evolution of the bulk modulus.

At the top surface, the structure is subjected to pure-mechanical transverse bi-sinusoidal load, reading:

$$p_z^+ = \hat{p}_z^+ \sin\left(\frac{m\ \pi\ \xi_1}{a} \right) \sin\left(\frac{n\ \pi\ \xi_2}{b} \right) \tag{21}$$

Here m,n are the wave numbers and a, b the plate/shell dimensions in the ξ_1, ξ_2 directions, respectively. A quantity with a superimposed hat denotes the amplitude of the respective load. $m = n = 1$ is assumed for the wave numbers

Since an analytical Navier-type solution is employed to assess the FEM results, the plate/shell is assumed to be simply supported. Due to the symmetry of both the load and the boundary conditions, only a quarter of the plate/shell is analyzed. Therefore, the following symmetry conditions and boundary conditions are applied:

$$\begin{aligned} &u = 0 \quad \text{at} \quad \xi_1 = 0, \\ &v = 0 \quad \text{at} \quad \xi_2 = 0, \\ &v = w = 0 \quad \text{at} \quad \xi_1 = a/2, \\ &u = w = 0 \quad \text{at} \quad \xi_2 = b/2, \end{aligned} \tag{22}$$

which are fulfilled by the assumed harmonic load.

As done in [35], non-dimensionalized quantities are introduced:

$$\bar{\boldsymbol{u}} = \frac{\boldsymbol{u}(\xi_3)}{P\ a}, \qquad \bar{\boldsymbol{\sigma}} = \frac{\boldsymbol{\sigma}(\xi_3)}{P\ B^*}, \tag{23}$$

where $P = \hat{p}_z^+ / B^*$ is taken for the applied load $p_z^+ = 1$ Pa. The scale factors is $B^* = 1$ GPa. The results are obtained using a square mesh $[8 \times 8]$, that is enough to obtain the convergence solution. The maximum value of the variables in the surface is considered in the following analysis.

7.1. Plate

A square plate with dimensions $a = b = 1$ is considered for this analysis. The thickness h is variable in order to consider different thickness ratios: $a/h = 4$, 10, 50. The exponential material index n_g is taken equal to 2, that allow us to take into account a quite high variability of FGM properties in the thickness direction.

In Tables 1 and 2 the FEM results, obtained with the different theories contained in the CUF, are compared with the 3D solution given by Reddy in [35]. The Table 1 shows the solution in terms of in-plane displacement $\bar{u}$ and transversal displacement $\bar{w}$ calculated at the top (t), middle (m) and bottom of the plate, while in Table 2 the stresses $\bar{\sigma}_{11}$, $\bar{\sigma}_{13}$ and $\bar{\sigma}_{33}$ are given. The results converge very well to the 3D solution by increasing the order of expansion N for both the displacements and the stresses, even when the plate is very thin ($a/h = 50$). One can conclude that the element does not suffer the shear locking and it is numerically robust and efficient. Only the normal stress present a larger error when the plate is very thin, even if an high order of expansion ($N = 4$) is used. But, this fact can be due to the small value of $\bar{\sigma}_{33}$ in respect to the in-plane stresses that makes difficult the numerical approximation. One can note that the FSDT provides good results only for the displacements (Table 1) in thin plates. For thick plates it fails because it does not consider the variability of the mechanical behavior in FGMs along the thickness. This is even more visible for the stresses in Table 2. Therefore, the FEM results confirm the conclusions made in [21], where the CUF analytical solution is calculated using the Navier method.

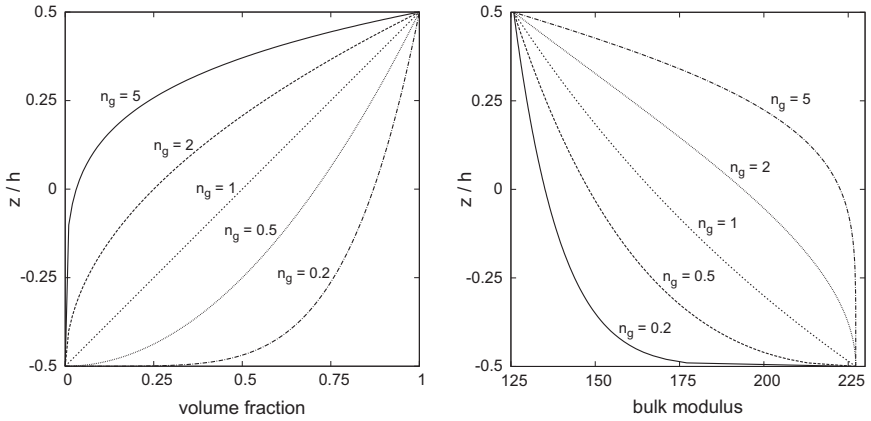

Fig. 3. Through-thickness distribution of the volume fraction V_c of the ceramic phase (left) and of the bulk modulus (right).

Table 1
Non-dimensional in-plane displacement $\bar{u}(\frac{a}{2},0)$ and transversal displacement $\bar{w}(0,0)$, calculated at the top (t), middle (m) and bottom (b) of the plate with material index $n_g = 2$.

	Ref. [35]	FSDT	$N = 1$	$N = 2$	$N = 3$	$N = 4$
	$a/h = 4$					
$\bar{u}_{(t)}$	4.021×10^{-3}	4.231×10^{-3}	4.072×10^{-3}	3.837×10^{-3}	4.025×10^{-3}	4.026×10^{-3}
$\bar{u}_{(m)}$	-8.998×10^{-5}	1.502×10^{-4}	-2.624×10^{-5}	-9.666×10^{-5}	-8.994×10^{-5}	-8.894×10^{-5}
$\bar{u}_{(b)}$	-4.069×10^{-3}	-3.931×10^{-3}	-4.125×10^{-3}	-3.878×10^{-3}	-4.069×10^{-3}	-4.071×10^{-3}
$\bar{w}_{(t)}$	1.346×10^{-2}	1.361×10^{-2}	1.406×10^{-2}	1.297×10^{-2}	1.347×10^{-2}	1.347×10^{-2}
$\bar{w}_{(m)}$	1.370×10^{-2}	1.361×10^{-2}	1.366×10^{-2}	1.325×10^{-2}	1.371×10^{-2}	1.371×10^{-2}
$\bar{w}_{(b)}$	1.273×10^{-2}	1.361×10^{-2}	1.326×10^{-2}	1.224×10^{-2}	1.274×10^{-2}	1.274×10^{-2}
	$a/h = 10$					
$\bar{u}_{(t)}$	2.617×10^{-2}	2.644×10^{-2}	2.619×10^{-2}	2.595×10^{-2}	$2.619 \cdot 10^{-2}$	2.619×10^{-2}
$\bar{u}_{(m)}$	7.108×10^{-4}	9.385×10^{-4}	6.644×10^{-4}	6.998×10^{-4}	7.157×10^{-4}	7.158×10^{-4}
$\bar{u}_{(b)}$	-2.472×10^{-2}	-2.456×10^{-2}	-2.486×10^{-2}	-2.450×10^{-2}	-2.473×10^{-2}	-2.473×10^{-2}
$\bar{w}_{(t)}$	0.1689	0.1704	0.1708	0.1675	0.1690	0.1690
$\bar{w}_{(m)}$	0.1707	0.1704	0.1706	0.1693	0.1707	0.1708
$\bar{w}_{(b)}$	0.1685	0.1704	0.1703	0.1671	0.1686	0.1686
	$a/h = 50$					
$\bar{u}_{(t)}$	0.6603	0.6610	0.6584	0.6588	0.6607	0.6607
$\bar{u}_{(m)}$	2.312×10^{-2}	2.346×10^{-2}	2.054×10^{-2}	2.297×10^{-2}	2.324×10^{-2}	2.324×10^{-2}
$\bar{u}_{(b)}$	−0.6141	−0.6141	−0.6173	−0.6128	−0.6142	−0.6142
$\bar{w}_{(t)}$	20.32	20.33	20.34	20.27	20.32	20.32
$\bar{w}_{(m)}$	20.33	20.33	20.34	20.28	20.33	20.34
$\bar{w}_{(b)}$	20.32	20.33	20.34	20.27	20.32	20.32

Table 2
Non-dimensional stresses $\bar{\sigma}_{11}(0,0), \bar{\sigma}_{13}(\frac{a}{2},0)$ and $\bar{\sigma}_{33}(0,0)$, calculated at the top (t), middle (m) and bottom (b) of the plate with material index $n_g = 2$.

	Ref. [35]	FSDT	$N = 1$	$N = 2$	$N = 3$	$N = 4$
	$a/h = 4$					
$\bar{\sigma}_{11(t)}$	3.154	2.877	3.048	2.863	3.225	3.166
$\bar{\sigma}_{11(m)}$	0.2037	0.1255	0.4607	0.3081	0.1978	0.2031
$\bar{\sigma}_{11(b)}$	−3.631	−3.519	−3.104	−3.654	−3.754	−3.648
$\bar{\sigma}_{13(m)}$	−0.9500	−0.6448	−0.6464	−0.6875	−0.9550	−0.9565
$\bar{\sigma}_{33(m)}$	0.5130	–	0.8654	0.7174	0.5036	0.5117
	$a/h = 10$					
$\bar{\sigma}_{11(t)}$	18.17	17.98	18.24	17.05	18.12	18.24
$\bar{\sigma}_{11(m)}$	0.8722	0.7842	1.305	1.507	0.8907	0.8818
$\bar{\sigma}_{11(b)}$	22.06	−21.99	−21.34	−22.99	−21.91	22.13
$\bar{\sigma}_{13(m)}$	−2.396	−1.612	−1.613	−1.745	−2.407	−2.406
$\bar{\sigma}_{33(m)}$	0.5142	–	2.014	1.701	0.5400	0.5233
	$a/h = 50$					
$\bar{\sigma}_{11(t)}$	447.9	449.4	452.2	423.1	444.3	449.9
$\bar{\sigma}_{11(m)}$	19.56	19.60	25.17	35.08	20.26	19.86
$\bar{\sigma}_{11(b)}$	−548.0	−549.7	−542.8	−573.5	−539.72	−549.5
$\bar{\sigma}_{13(m)}$	−12.00	−8.068	−8.070	−8.756	−12.06	−12.05
$\bar{\sigma}_{33(m)}$	0.5141	–	34.28	29.32	1.553	0.8030

Table 3
Non-dimensional in-plane displacement $\bar{u}(\frac{a}{2},0)$ and transversal displacement $\bar{w}(0,0)$, calculated at the top (t), middle (m) and bottom (b) of the shell with material index $n_g = 2$.

	Ref. [22]	FSDT	$N = 1$	$N = 2$	$N = 3$	$N = 4$
	$R/h = 10$					
$\bar{u}_{(t)}$	0.0012	1.048×10^{-3}	7.937×10^{-4}	6.659×10^{-4}	1.089×10^{-3}	1.152×10^{-3}
$\bar{u}_{(m)}$	−0.0006	-2.562×10^{-6}	-2.589×10^{-4}	-6.100×10^{-4}	-6.251×10^{-4}	-5.739×10^{-4}
$\bar{u}_{(b)}$	−0.0010	-1.053×10^{-3}	-1.311×10^{-3}	-5.911×10^{-4}	-9.708×10^{-3}	-1.004×10^{-3}
$\bar{w}_{(t)}$	0.0039	2.338×10^{-3}	3.503×10^{-3}	3.499×10^{-3}	3.835×10^{-3}	3.876×10^{-3}
$\bar{w}_{(m)}$	0.0021	2.338×10^{-3}	2.327×10^{-3}	1.950×10^{-3}	2.158×10^{-3}	2.126×10^{-3}
$\bar{w}_{(b)}$	0.0013	2.338×10^{-3}	1.152×10^{-3}	9.847×10^{-4}	1.306×10^{-3}	1.331×10^{-3}
	$R/h = 100$					
$\bar{u}_{(t)}$	0.0881	0.0887	0.0900	0.0876	0.0881	0.0881
$\bar{u}_{(m)}$	−0.0035	−0.0031	−0.0021	−0.0035	−0.0035	−0.0035
$\bar{u}_{(b)}$	−0.0952	−0.0949	−0.0943	−0.0946	−0.0951	−0.0951
$\bar{w}_{(t)}$	0.5984	0.5993	0.6006	0.5912	0.5944	0.5944
$\bar{w}_{(m)}$	0.5992	0.5993	0.6010	0.5956	0.5988	0.5989
$\bar{w}_{(b)}$	0.5964	0.5993	0.6015	0.5927	0.5960	0.5960
	$R/h = 1000$					
$\bar{u}_{(t)}$	0.3157	0.3168	0.4970	0.3157	0.3163	0.3163
$\bar{u}_{(m)}$	−0.5553	−0.5547	−0.4285	−0.5551	−0.5549	−0.5549
$\bar{u}_{(b)}$	−1.426	−1.426	−1.354	−1.426	−1.426	−1.426
$\bar{w}_{(t)}$	55.45	55.50	58.92	55.44	55.47	55.47
$\bar{w}_{(m)}$	55.46	55.50	58.93	55.46	55.48	55.49
$\bar{w}_{(b)}$	55.47	55.50	58.94	55.46	55.49	55.49

Table 4
Non-dimensional stresses $\bar{\sigma}_{22}(0,0), \bar{\sigma}_{13}(\frac{a}{2},0)$ and $\bar{\sigma}_{33}(0,0)$, calculated at the top (t), middle (m) and bottom (b) of the shell with material index $n_g = 2$.

	Ref. [22]	FSDT	$N = 1$	$N = 2$	$N = 3$	$N = 4$
	$R/h = 10$					
$\bar{\sigma}_{22(t)}$	0.6770	0.2091	0.3929	0.5808	0.7466	0.6909
$\bar{\sigma}_{22(m)}$	0.1571	0.0439	0.3405	0.1365	0.1397	0.1602
$\bar{\sigma}_{22(b)}$	−0.2194	−0.2149	−0.1294	−0.0717	−0.3768	−0.2043
$\bar{\sigma}_{13(m)}$	−0.4440	−0.3347	−0.3322	−0.3107	−0.4521	−0.4574
$\bar{\sigma}_{33(m)}$	0.4486	–	0.5630	0.4346	0.4390	0.4570
	$R/h = 100$					
$\bar{\sigma}_{22(t)}$	24.32	24.19	23.63	22.34	24.14	24.45
$\bar{\sigma}_{22(m)}$	11.03	10.88	9.794	12.22	11.07	11.05
$\bar{\sigma}_{22(b)}$	−11.22	−11.26	−12.68	−13.42	−10.82	−11.35
$\bar{\sigma}_{13(m)}$	−4.324	−2.910	−2.920	−3.147	−4.343	−4.339
$\bar{\sigma}_{33(m)}$	0.4689	–	5.419	2.757	0.5206	0.4802
	$R/h = 1000$					
$\bar{\sigma}_{22(t)}$	955.9	958.8	916.0	932.8	955.5	959.0
$\bar{\sigma}_{22(m)}$	945.9	948.7	822.0	965.3	949.1	948.9
$\bar{\sigma}_{22(b)}$	780.1	781.9	600.4	748.6	788.2	782.2
$\bar{\sigma}_{13(m)}$	−3.862	−2.594	−2.775	−2.792	−3.878	−3.874
$\bar{\sigma}_{33(m)}$	0.4784	–	260.7	32.14	1.155	0.6914

7.2. Shell

Referring to Fig. 1, a shell with the following geometrical data is considered:

$$a = L = 1\ \text{m}, \quad b = \frac{\pi}{3}R, \quad R = 10\ \text{m}, \tag{24}$$

and different thickness ratios are taken: $R/h = 10, 100, 1000$. Also for the shell, the material index is $n_g = 2$.

Table 3 shows the results in terms of displacements $\bar{u}$ and $\bar{w}$ and Table 4 in terms of the stresses $\bar{\sigma}_{22}$, $\bar{\sigma}_{13}$ and $\bar{\sigma}_{33}$. In this case, the reference solution is given in [22]. It is obtained using a fourth-order CUF theory and taking a very high number of fictitious layers ($N_l = 150$) in the FGM shell, in which the mechanical properties are considered constant along the thickness and equal to the mean value between the top and bottom of the layer. In [22], it has been demonstrated that this procedure permits to calculate the quasi-3D solution of the static problem in FGM structures. The comparison of FEM results with the quasi-3D solution shows that the CUF element works very well also for the shell and it confirms the conclusions made for the plate. A fourth-order of expansion of the displacement field in the thickness direction is necessary to ensure the convergence. The element provides very good results also for very thin shells ($R/h = 1000$) in spite of the membrane and shear locking phenomenon that usually affects the shell finite elements. As for the plate, the FSDT model is not able to accurately describe the distribution of displacements and stresses along the thickness in FGM shells.

As discussed in [22], the influence of the material gradient on the variation of the transversal displacement is more evident in the thermal analysis and the use of higher-order models becomes mandatory in that case. For these reasons, a future companion work will be dedicated to the thermal analysis of functionally graded plates and shells by means of the CUF shell element.

8. Conclusions

A shell finite element based on Carrera's Unified Formulation for the mechanical analysis of FGM plates and shells has been presented in this work. The element has cylindrical geometry and the MITC technique has been adopted to withstand the membrane and shear locking phenomenon. The governing equations are derived from the PVD and the grading material variation in the thickness direction is taken into account. Both a plate and a shell are considered for the analysis. They are simply supported and subjected to a bi-sinusoidal pressure load. These conditions permit to calculate the quasi-3D analytical solution of the problem by means of the Navier method and higher-order models. The comparison of the FEM results with the reference solutions show that the shell element provides very accurate results for both the plate and the shell. The locking phenomenon does not appear, even if the considered structure is very thin. The use of higher-order expansions is necessary to correctly describe the distribution of displacements and stresses along the thickness in functionally graded plates and shells. It is demonstrated that the assumption of constant transversal displacement, on which the FSDT is based, is not valid in FGMs.

Acknowledgment

Authors acknowledge the partial support of Piemonte Regional Project STEPS.

Appendix A

The explicit expression of the fundamental nucleus $\boldsymbol{K}^{\tau s\ ij}$ is proposed below.

Introducing the following notation:

$$\lhd(\cdot)\rhd_\Omega = \int_\Omega (\cdot)\, d\Omega, \quad \lhd(\cdot)\rhd_A = \int_A (\cdot) H\, d\xi_3,$$

the fundamental nucleus $K^{\tau s\ i\ j}$ can be written as:

$$\begin{aligned}
K_{11}^{\tau sij} &= N_{i_{m1}} \lhd N_{m1} N_{n1} \rhd_\Omega N_{j_{n1}} \lhd C_{44} F_{\tau,3} F_{s,3} \rhd_A + \\
&\quad N_{i,1_{m1}} \lhd N_{m1} N_{n1} \rhd_\Omega N_{j,1_{n1}} \lhd C_{11} F_\tau F_s \rhd_A + \\
&\quad N_{i,2_{m3}} \lhd N_{m3} N_{n3} \rhd_\Omega N_{j,2_{n3}} \lhd C_{44} F_\tau F_s \rhd_A
\end{aligned} \tag{25}$$

$$\begin{aligned}
K_{12}^{\tau sij} &= N_{i,1_{m1}} \lhd N_{m1} N_{n2} \rhd_\Omega N_{j,2_{n2}} \lhd C_{12} H F_\tau F_s \rhd_A + \\
&\quad N_{i,2_{m3}} \lhd N_{m3} N_{n3} \rhd_\Omega N_{j,1_{n3}} \lhd C_{44} H F_\tau F_s \rhd_A
\end{aligned}$$

$$\begin{aligned}
K_{13}^{\tau sij} &= N_{i,1_{m1}} \lhd N_{m1} N_j \rhd_\Omega \lhd C_{12} F_\tau F_{s,3} \rhd_A + \\
&\quad \frac{1}{R} N_{i,1_{m1}} \lhd N_{m1} N_{n2} \rhd_\Omega N_{j_{n2}} \lhd C_{12} H F_\tau F_s \rhd_A + \\
&\quad N_{i_{m1}} \lhd N_{m1} N_{n1} \rhd_\Omega N_{j,1_{n1}} \lhd C_{44} F_{\tau,3} F_s \rhd_A
\end{aligned}$$

$$\begin{aligned}
K_{21}^{\tau sij} &= N_{i,2_{m2}} \lhd N_{m2} N_{n1} \rhd_\Omega N_{j,1_{n1}} \lhd C_{12} H F_\tau F_s \rhd_A + \\
&\quad N_{i,1_{m3}} \lhd N_{m3} N_{n3} \rhd_\Omega N_{j,2_{n3}} \lhd C_{44} H F_\tau F_s \rhd_A
\end{aligned}$$

$$\begin{aligned}
K_{22}^{\tau sij} &= N_{i,2_{m2}} \lhd N_{m2} N_{n2} \rhd_\Omega N_{j,2_{n2}} \lhd C_{11} H^2 F_\tau F_s \rhd_A + \\
&\quad N_{i,1_{m3}} \lhd N_{m3} N_{n3} \rhd_\Omega N_{j,1_{n3}} \lhd C_{44} H^2 F_\tau F_s \rhd_A + \\
&\quad \frac{1}{R^2} N_{i_{m2}} \lhd N_{m2} N_{n2} \rhd_\Omega N_{j_{n2}} \lhd C_{44} F_\tau F_s \rhd_A - \\
&\quad \frac{1}{R} N_{i_{m2}} \lhd N_{m2} N_{n2} \rhd_\Omega N_{j_{n2}} \lhd C_{44} H F_\tau F_{s,3} \rhd_A - \\
&\quad \frac{1}{R} N_{i_{m2}} \lhd N_{m2} N_{n2} \rhd_\Omega N_{j_{n2}} \lhd C_{44} H F_{\tau,3} F_s \rhd_A + \\
&\quad N_{i_{m2}} \lhd N_{m2} N_{n2} \rhd_\Omega N_{j_{n2}} \lhd C_{44} H^2 F_{\tau,3} F_{s,3} \rhd_A
\end{aligned} \tag{26}$$

$$\begin{aligned}
K_{23}^{\tau sij} &= \frac{1}{R} N_{i,2_{m2}} \lhd N_{m2} N_{n2} \rhd_\Omega N_{j_{n2}} \lhd C_{11} H^2 F_\tau F_s \rhd_A + \\
&\quad N_{i,2_{m2}} \lhd N_{m2} N_j \rhd_\Omega \lhd C_{12} H F_\tau F_{s,3} \rhd_A - \\
&\quad \frac{1}{R} N_{i_{m2}} \lhd N_{m2} N_{n2} \rhd_\Omega N_{j,2_{n2}} \lhd C_{44} F_\tau F_s \rhd_A + \\
&\quad N_{i_{m2}} \lhd N_{m2} N_{n2} \rhd_\Omega N_{j,2_{n2}} \lhd C_{44} H F_{\tau,3} F_s \rhd_A
\end{aligned}$$

$$\begin{aligned}
K_{31}^{\tau sij} &= N_{i,1_{m1}} \lhd N_{m1} N_{n1} \rhd_\Omega N_{j_{n1}} \lhd C_{44} F_\tau F_{s,3} \rhd_A + \\
&\quad \frac{1}{R} N_{i_{m2}} \lhd N_{m2} N_{n1} \rhd_\Omega N_{j,1_{n1}} \lhd C_{12} H F_\tau F_s \rhd_A + \\
&\quad \lhd N_i N_{n1} \rhd_\Omega N_{j,1_{n1}} \lhd C_{12} F_{\tau,3} F_s \rhd_A
\end{aligned}$$

$$\begin{aligned}
K_{32}^{\tau sij} &= \frac{1}{R} N_{i_{m2}} \lhd N_{m2} N_{n2} \rhd_\Omega N_{j,2_{n2}} \lhd C_{11} H^2 F_\tau F_s \rhd_A + \\
&\quad \lhd N_i N_{n2} \rhd_\Omega N_{j,2_{n2}} \lhd C_{12} H F_{\tau,3} F_s \rhd_A - \\
&\quad \frac{1}{R} N_{i,2_{m2}} \lhd N_{m2} N_{n2} \rhd_\Omega N_{j_{n2}} \lhd C_{44} F_\tau F_s \rhd_A + \\
&\quad N_{i,2_{m2}} \lhd N_{m2} N_{n2} \rhd_\Omega N_{j_{n2}} \lhd C_{44} H F_\tau F_s \rhd_A
\end{aligned}$$

$$\begin{aligned}
K_{33}^{\tau sij} &= \frac{1}{R^2} N_{i_{m2}} \lhd N_{m2} N_{n2} \rhd_\Omega N_{j_{n2}} \lhd C_{11} H^2 F_\tau F_s \rhd_A + \\
&\quad \frac{1}{R} N_{i_{m2}} \lhd N_{m2} N_j \rhd_\Omega \lhd C_{12} H F_\tau F_{s,3} \rhd_A + \\
&\quad \frac{1}{R} \lhd N_i N_{n2} \rhd_\Omega N_{j_{n2}} \lhd C_{12} H F_{\tau,3} F_s \rhd_A + \\
&\quad \lhd N_i N_j \rhd_\Omega \lhd C_{11} F_{\tau,3} F_{s,3} \rhd_A + \\
&\quad N_{i,1_{m1}} \lhd N_{m1} N_{n1} \rhd_\Omega N_{j,1_{n1}} \lhd C_{44} F_\tau F_s \rhd_A + \\
&\quad N_{i,2_{m2}} \lhd N_{m2} N_{n2} \rhd_\Omega N_{j,2_{n2}} \lhd C_{44} F_\tau F_s \rhd_A
\end{aligned} \tag{27}$$

Both the integrals in the surface and in the thickness direction are calculated using the Gaussian quadrature rule.

References

[1] Tanigawa Y. Some basic thermoelastic problems for nonhomogeneous structural materials. Appl Mech Rev 1995;48:287–300.
[2] Koizumi M. The concept of FGM. Ceram Trans Funct Graded Mater 1993;34:3–10.
[3] Suresh S, Mortensen A. Fundamentals of Functionally Graded Materials. London: IOM Communications Ltd.; 1998.
[4] Wetherhold RC, Wang SS. The use of functionally graded materials to eliminate or control thermal deformation. Compos Sci Technol 1996;56:1099–104.
[5] Kashtalyan M. Three-dimensional elasticity solution for bending of functionally graded rectangular plates. Eur J Mech A/Solids 2004;23(5): 853–64.
[6] Vel SS, Baskiyar R. Thermally induced stresses in functionally graded thick tubes. In: AIP conference proceedings; vol. 973, 2008. p. 688–93.
[7] Abrinia K, Naee H, Sadeghi F, Djavanroodi F. New analysis for the FGM thick cylinders under combined pressure and temperature loading. Am J Appl Sci 2008;5(7):852–9.
[8] Chi S-H, -L Chung Y. Mechanical behavior of functionally graded material plates under transverse load. Part I: Analysis. Int J Solids Struct 2006;43(13): 3657–74.
[9] Zenkour AM. Generalized shear deformation theory for bending analysis of functionally graded plates. Appl Math Modell 2006;30(1):67–84.
[10] Batra RC, Jin J. Natural frequencies of a functionally graded anisotropic rectangular plate. J Sound Vib 2005;282(1–2):509–16.
[11] Dai KY, Liu GR, Lim KM, Han X, Y Du S. A meshfree radial point interpolation method for analysis of functionally garded material (FGM) plates. Comput Mech 2004;34:213–23.
[12] Pelletier JL, Vel SS. An exact solution for the steady-state thermoelastic response of functionally graded orthotropic cylindrical shells. Int J Solids Struct 2006;43:1131–58.
[13] Chinosi C, Della Croce L. Mixed-interpolated finite elements for functionally graded cylindrical shells. Compos Struct 2010;92:2314–20.
[14] Ramirez F, Heyliger PR, Pan E. Static analysis of functionally graded elastic anisotropic plates using a discrete layer approach. Compos Part B: Eng 2006;37(1):10–20.
[15] Shao ZS, Wang TJ. Three-dimensional solutions for the stress fields in functionally graded cylindrical panel with finite length and subjected to thermal/mechanical loads. Int J Solids Struct 2006;43:3856–74.
[16] Ferreira AJM, Batra RC, Roque CMC, Qian LF, Martins PALS. Static analysis of functionally graded plates using third-order shear deformation theory and a meshless method. Compos Struct 2005;69(4):449–57.
[17] Qian LF, Batra RC, Chen LM. Static and dynamic deformations of thick functionally graded elastic plates by using higher-order shear and normal deformable plate theory and meshless local Petrov–Galerkin method. Compos Part B: Eng 2004;35(6–8):685–97.
[18] Athuri SN, Zhu T. A new meshless Local Petrov–Galerkin (MLPG) approach in computational mechanics. Comput Mech 1998;22:117–27.
[19] Carrera E. A class of two dimensional theories for multilayered plates analysis. Atti Accademia delle Scienze di Torino, Mem Sci Fis 1995;19–20:49–87.
[20] Carrera E, Brischetto S, Robaldo A. A variable kinematic model for the analysis of Functionally Graded Materials plates. AIAA J 2008;46:194–203.
[21] Brischetto S, Leetsch R, Carrera E, Wallmersrerger T, Kröplin B. Thermo-machanical bending of functionally graded plates. J Thermal Stress 2008;31(3):286–308.
[22] Cinefra M, Carrera E, Brischetto S, Belouettar S. Thermo-machanical analysis of functionally graded shells. J Thermal Stress 2010;33:942–63.
[23] Cinefra M, Soave M. Accurate vibration analysis of multilayered plates made of functionally graded materials. Mech Ada Mater Struct 2011;18(1):3–13.
[24] Cinefra M, Belouettar S, Soave M, Carrera E. Variable kinematic models applied to free vibration analysis of functionally graded material shells. Eur J Mech. A, Solids 2010;29:1078–87.
[25] Brischetto S, Carrera E. Advanced mixed theories for bending analysis of functionally graded plates. Comput Struct 2008;88:1474–83.
[26] Carrera E, Brischetto S, Cinefra M, Soave M. Refined and advanced models for multilayered plates and shells embedding functionally graded material layers. Mech Adv Mater Struct 2010;19:604–22.

[27] He XQ, Liew KM, Ng TY, Sivashanker S. Active control of FGM plates subjected to a temperature gradient: modeling via finite element method based on FSDT. Int J Numer Methods Eng 2001;52:1253–71.
[28] Liew KM, He XQ, Kitipornchai S. Finite element method for the feedback control of FGM shells in the frequency domain via piezoelectric sensors and actuators. Comput Methods Appl Mech Eng 2004;193:257–73.
[29] Reddy JN, Chin CD. Thermomechanical analysis of functionally graded cylinders and plates. J Thermal Stress 1988;21:593–626.
[30] Carrera E. Theories and finite elements for multilayered plates and shells: a unified compact formulation with numerical assessment and benchmarking. Arch Comput Methods Eng 2003;10(3):215–96.
[31] Chapelle D, Bathe K-J. The Finite Element Analysis of Shells. – Fundamentals. Berlin: Springer; 2003.
[32] Cinefra M, Chinosi C, Della Croce L. MITC9 shell elements based on refined theories for the analysis of isotropic cylindrical structures. Mech Adv Mater Struct, accepted for publication.
[33] Bathe K-J, Dvorkin E. A formulation of general shell elements – the use of mixed interpolation of tensorial components. Int J Numer Methods Eng 1986;22:697–722.
[34] Bucalem ML, Bathe K-J. Higher-order MITC general shell elements. Int J Numer Methods Eng 1993;36:3729–54.
[35] Reddy JN, Chen ZN. Three-dimensional thermomechanical deformations of functionally graded rectangular plates. Eur J Mech A/Solids 2001;20(5):841–55.
[36] Mori T, Tanaka K. Average stress in matrix and average elastic energy of materials with misfitting inclusions. Acta Metall 1973;21:571–4.
[37] Benveniste Y. A new approach to the application of Mori–Tanaka's theory in composite materials. Mech Mater 1987;6:147–57.